JOURNAL OF MATERIALS SCIENCE 30(1995) 737–743

Thermal decomposition of the Pb, Al-hydrotalcite material

M. L. VALCHEVA-TRAYKOVA, N. DAVIDOVA
Institute of Kinetics and Catalysis, Bulgarian Academy of Sciences, 11 G. Bonchev Street, Sofia 1040, Bulgaria

A. H. WEISS
Department of Chemical Engineering, Worcester Polytechnic Institute, 100 Institute Road, Worcester, MA 01609, USA

The transformation of methane into C_2 hydrocarbons over thermally degraded Mg, Pb, Al-hydrotalcite material proceeds with the active participation of β-PbO. The conditions of pre-treatment leading β-PbO formation in the catalyst have been examined on the Pb, Al-hydrotalcite material as a model system. By use of X-ray diffraction, scanning electron microscopy, transmission electron microscopy, infrared spectroscopy and diffuse-reflectance spectroscopy techniques, it was found that the temperature interval 600–750 °C is optimal for β-PbO crystallization. On the basis of the present and previous results, the formation of all components of the catalytically active thermally degraded Mg, Pb, Al-hydrotalcite material, has been explained. During calcination of the Mg, Pb, Al-hydrotalcite material, the lead-containing components form β-PbO and γ-Al_2O_3 and the magnesium-containing components transform to a finely dispersed MgO-Al_2O_3 matrix.

1. Introduction

Lead oxide participates in the electron transfer during oxidative coupling of methane over several lead oxide-containing catalysts [1]. It is assumed that Pb^{2+} is active in the formation of the $CH_3^{\cdot}$ radicals on the catalytic surface [1, 2]. The 750 °C calcined Mg, Pb, Al-hydrotalcite material is reported [2] to be a good catalyst for oxidative dimerization of methane. In the X-ray diffraction (XRD) pattern of the activated catalyst, α- and β-PbO are detected in the highly dispersed matrix of MgO and γ-Al_2O_3. The β-PbO is assumed to be the most active lead oxide phase in the oxygen transfer in the partial oxidation of methane to ethane over the 750 °C calcined Mg, Pb, Al-hydrotalcite material. During the reaction, PbO transformed into lead, which on interaction with the gaseous oxygen, deoxidized to β-PbO. The deactivated catalyst contained metallic lead in a highly dispersed MgO–Al_2O_3 matrix. After regeneration, lead transformed to β-PbO and significant reflections of α-Al_2O_3 appeared in the X-ray diffraction pattern of the sample.

In the present work, the effect of the thermal treatment on the solid–solid phase transitions of the model Pb, Al-hydrotalcite material was investigated, to determine the conditions of calcination leading to β-PbO crystallization. The next purpose, on the basis of the present and previous [3] investigations, was to clarify the role of the lead and magnesium components in the formation of the catalytically active methane dimerization mixed oxide system by calcination of Mg, Pb, Al-hydrotalcite material at 750 °C. The model system contained only lead and aluminium and was synthesized by the procedure used for the synthesis of the Mg, Pb, Al-hydrotalcite material [4].

2. Experimental procedure

2.1. Preparation of the material

The sample was prepared to contain Me^{2+}:Me^{3+} atomic ratio typical for the hydrotalcite (at about 2), using the hydrotalcite preparation procedure that avoids filtering and washing problems associated with gel precipitates [4]. First, 82.75 g $Pb(NO_3)_2 \cdot 24H_2O$ (p.a.) and 47 g $Al(NO_3)_3 \cdot 9H_2O$ (p.a.) were dissolved in 350 ml de-ionized water. Separately, 35 g NaOH were dissolved with 175 ml de-ionized water in a teflon container. Then 25 g Na_2CO_3 were dissolved in de-ionized water and added to the NaOH solution in the teflon reactor. The Pb, Al solution was added to the reactor by strong mixing using a teflon stirrer, for 18 h at 32 °C. Then the temperature in the reactor was increased to 65 °C and the material was vigorously mixed at this temperature for 18 h. The vessel was removed from both mixing and heat treatment and placed in an ice bath to quench the reaction. The slurry was then suction filtered, washed and dried at 120 °C in a furnace for 24 h. The large ionic radius of Pb^{2+} determines the small probability of the formation of lead-containing hydrotalcite phase. No data have been found in the literature on this subject; but because it was prepared by the hydrotalcite synthesize procedure, it was named "Pb, Al-hydrotalcite

material". In the present work, the probability of the formation of some amount of lead-containing hydrotalcite was not rejected a priori, but investigated by X-ray diffraction, TEM, SEM, and other techniques and statistically verified.

2.2. X-ray diffraction

The X-ray diffraction (XRD) analysis was performed using a General Electric XRD-5 Diffractometer, at CuK_α irradiation, and a nickel filter, in the range $2\theta = 5°$–$90°$, 2θ rate $4° \text{ min}^{-1}$. The position of the maximum of each reflection in the X-ray diffraction pattern was detected automatically. Phase analysis was performed using the procedure described elsewhere [5–9]. The existence of each phase was examined by calculation of its unit cell parameters. The precise determination of the unit cell parameters is based on calculation of their values using characteristic d-spacings and approximation of the Nelson–Railly function $a = f(\theta)$ to $\theta = 90°$ [10]. The reliability of the Nelson–Railly function is estimated by correlation analysis. The correlation coefficient, r_{yx}, for each unit cell parameter has been calculated [11]. If $r_{yx} = 1$, a linear relationship exists between $f(\theta)$ and the unit cell parameter (a_0 or c_0). A value of $r_{yx} \neq 1$ indicates statistical control of the significance of the functional relationship between $f(\theta)$ and a_0 (or c_0). In this case the correlation coefficient, r_{yx}, calculated from the experimental data shoud be compared with its corresponding critical value, $r_{yx}(\alpha, f)$; where α is the level of significance, and $f = N - 2$ (N being the number of the parallel observations) is the number of degrees of freedom. In our investigations, the critical value of the correlation coefficient is $r_{yx}(\alpha, f) = 0.754$ [11]. If $r_{yx} > r_{yx}(\alpha, f)$, the relationship between $f(\theta)$ and the unit cell parameter is statistically significant, reliable, and can be described by polynomes of the first or second order [11].

2.3. Scanning electron microscopy

The scanning electron micrographs were recorded using a T-200 SEM at electron microscopic magnifications of 100–10 000, and photographic magnifications 1×2.

2.4. Transmission electron microscopy

TEM investigations were performed with a JEM-100 at $U = 80$ kV. A water suspension of finely dispersed powder of the Pb, Al-hydrotalcite material was prepared and investigated under "white-field" conditions at electron microscopic magnifications of 20 000, 30 000, 35 000, 50 000, 60 000, 70 000, 75 000, 80 000 and 100 000. The largest populations of particles observed were detected photographically and developed at photographic magnification 4×1.

2.5. Infrared (IR) spectroscopy

IR spectra were recorded using a Bruker "IFS 113 V" Fourier Transform Infrared Spectrometer in the range 4000–400 cm^{-1} (standard error $\pm$ 1 cm^{-1}) in tablets, in air. About 0.0004 $\pm$ 0.00005 g of the sample were mixed in 0.200 g KBr (p.a.) and used to form tablets with surface of 1 cm^2. Characteristic vibration data of the hydrotalcite structure [12, 13] and of other components of the hydrotalcite material [9] have been used in the interpretation. The characteristic vibrations of the structural OH groups, as well as of the water molecules and water complexes of the metal ions in the zeolite lattice were seen in the region 4000–3000 cm^{-1}. Their interpretation is possible only using the information from the diffuse-reflectance spectra.

2.6. Diffuse-reflectance spectroscopy (DRS)

The diffuse-reflectance spectra were recorded using a Beckman apparatus in the range 50 000–4000 cm^{-1}. The pure material was dried at 120 °C in a furnace for 24 h and cooled to room temperature in a desiccator, in the presence of blau-gel. Then tablets containing about 0.2 g of the material were prepared. As standard, tablets of $BaSO_4$ (p.a.) were used. The fundamental stretching vibrations, $\nu_{0\to1}$, and their first $\nu_{0\to2}$ overtones, were calculated using the method described elsewhere [14–16].

3. Results

3.1. XRD

In the X-ray diffraction pattern of the uncalcined Pb, Al-hydrotalcite material (Fig. 1), reflections characteristic of dandassite $PbAl_2(CO_3)_4 \cdot 2H_2O$, hydrocerrussite $Pb_3(CO_3)_2(OH)_2$ and $Al(OH)_3$ gibbsite and bayerite, are seen. Weak and sharp reflections of hydrotalcite are also observed ($d_{003} = 0.682$ nm, $d_{006} = 0.3787$ nm, $d_{101} = 0.2616$ nm, $d_{104} = 0.2443$ nm, $d_{015} = 0.2311$ nm, $d_{107} = 0.2072$ nm, $d_{1010} = 0.1732$ nm, $d_{113} = 0.1507$ nm, $d_{116} = 0.1425$ nm). The approximation of the linear Nelson–Railly function to $\theta = 90°$ gives a slope for $a_0 = 0.30971$ nm ($r_{yx} = 0.9760$; standard deviation $\sigma = 0.002\,58$) and for $c_0 = 2.191\,96$ nm ($r_{yx} = 0.9258$; standard deviation $\sigma = 0.037\,95$). The corresponding critical value of r_{yx} (0.05, 5) is 0.754 [11]. The correlation coefficients $r_{yx} > 0.754$ for both unit cell parameters confirm the statistical significance and reliability of the linear

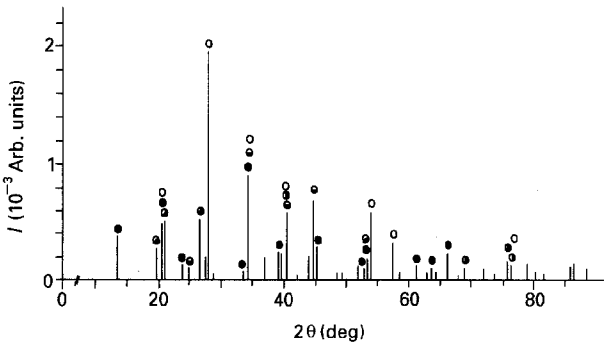

Figure 1 X-ray diffraction pattern of the uncalcined Pb, Al-hydrotalcite material: (●) hydrotalcite, (◒) $Pb_3(CO_3)2(OH)_2$, (◑) $PbAl_2(CO_3)_4 2H_2O$, (○) $Al(OH)_3$ bayerite, (◑) $Al(OH)_3$ gibbsite.

TABLE I Millers' indexes ($h\,k\,l$), experimentally detected d-spacings $d_{h\,k\,l}$, experimental ("exp") and theoretical ("calc") values of the unit cell parameters, a_0 and c_0, of the hydrotalcite structure

($h\,k\,l$)	$d_{h\,k\,l}$ (nm)	a_{0exp} (nm)	a_{0calc} (nm)	c_{0exp} (nm)	c_{0calc} (nm)
003	0.6820	–	–	–	–
006	0.3787	–	–	–	–
101	0.2616	0.309 00 ± 0.0006	0.307 32	2.363 64 ± 1.5444	2.346 20
104	0.2443	0.306 75 ± 0.0004	0.307 51	2.339 18 ± 2.1207	2.333 70
015	0.2311	0.312 25 ± 0.0075	0.307 66	2.324 22 ± 1.1744	2.324 22
107	0.2072	0.308 73 ± 0.0050	0.307 93	2.291 16 ± 1.4358	2.306 65
1010	0.1732	0.308 74 ± 0.0051	0.308 30	2.270 30 ± 1.2196	2.283 11
113	0.1507	0.308 96 ± 0.0052	0.308 62	2.268 42 ± 1.8650	2.262 42
116	0.1425	0.306 74 ± 0.0059	0.308 72	2.268 42 ± 1.7650	2.255 81

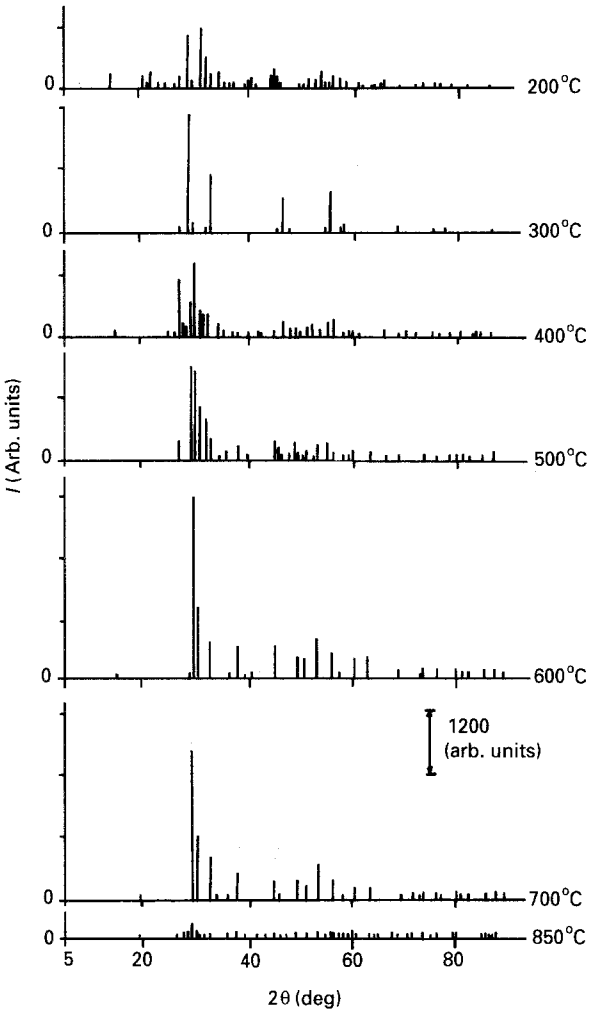

Figure 2 X-ray diffraction patterns of the Pb, Al-hydrotalcite material after calcination at 200–850 °C.

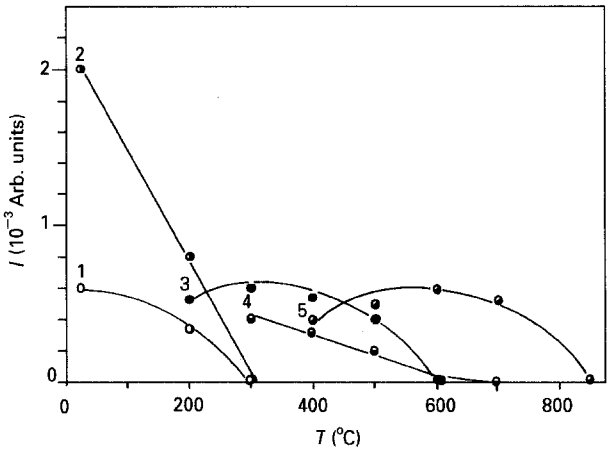

Figure 3 Relative changes in the intensities of the characteristic reflections of the (1, ○), gibbsite, (2, ◑) bayerite, (3, ●) boehmite, (4, ◒) α-Al_2O_3, and (5, ◭) γ-Al_2O_3 in the X-ray diffraction pattern of the Pb, Al-hydrotalcite material after calcination at 200–850 °C.

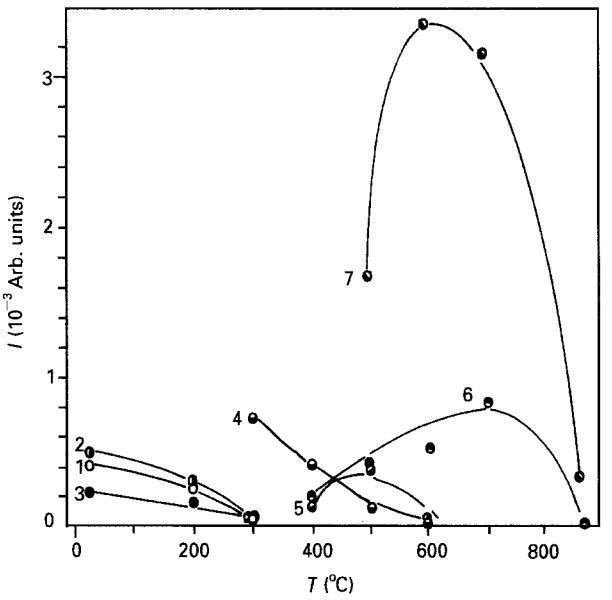

Figure 4 Relative changes in the intensities of the characteristic reflections of (1, ○) hydrotalcite, (2, ◑) hydrocerrussite, (3, ●) dandassite, (4, ◒) Pb_3O_4, (5, ◭) PbO_2, (6, ◓) α-PbO, and (7, ◒) β-PbO in the X-ray diffraction patterns of the Pb, Al-hydrotalcite material after calcination at temperatures between 200 and 850 °C.

relationship between $f(\theta)$ and unit cell parameters. The d-spacings registered d_{hkl}, their corresponding Miller's indexes ($h\,k\,l$), and the experimental and theoretical values of the unit cell parameters, a_0 and c_0, are given in Table I. The low intensities of the hydrotalcite reflections can be related to the small amount of this compound, in agreement with the small probability to form hydrotalcite structure with the participation of the Pb^{2+} ion with a large radius.

Several solid–solid phase transitions are registered after calcination of the material at 200–850 °C (Fig. 2). After calcination at 200 °C the characteristic reflections of the two polymorphous forms of $Al(OH)_3$ relatively decrease (Fig. 3, curves 1, 2) and characteristic reflections of boehmite appear (Fig. 3, curve 3). The reflections of all lead-containing components of the material also relatively decrease (Fig. 4, curves 1–3). After calcination at 300 °C the characteristic

reflections of the lead-containing hydroxycarbonates (Fig. 4, curves 1–3), of the gibbsite (Fig. 3, curve 1) and bayerite (Fig. 3, curve 2), disappear. The reflections of the boehmite relatively increase (Fig. 3, curve 3) and characteristic reflections of α-Al_2O_3 (Fig. 3, curve 4) and Pb_3O_4 (Fig. 4, curve 4) appear. At 400 °C, the intensities of the boehmite (Fig. 3, curve 3) and Pb_3O_4 (Fig. 4, curve 4) decrease. Three new phases are formed at this temperature: γ-Al_2O_3 (Fig. 3, curve 5), α-PbO (Fig. 4, curve 6) and PbO_2 (Fig. 4, curve 5). After calcination at 500 °C, sharp and intensive characteristic reflections of β-PbO can be seen in the XRD pattern of the Pb, Al-hydrotalcite material (Fig. 4, curve 7). The intensities of the γ-Al_2O_3 (Fig. 3, curve 5), α-PbO (Fig. 4, curve 5) and PbO_2 (Fig. 4, curve 6) significantly increase, while those of Pb_3O_4 (Fig. 4, curve 4), boehmite (Fig. 3, curve 3) and α-Al_2O_3 (Fig. 3, curve 4) significantly decrease. At 600 °C the boehmite, α-Al_2O_3, Pb_3O_4 and PbO_2 characteristic reflections disappear. The characteristic reflections of the γ-Al_2O_3 (Fig. 3, curve 5) and of the β-PbO (Fig. 4, curve 7) became most intensive. At 700 °C the characteristic reflections of the γ-Al_2O_3 decrease insignificantly (Fig. 3, curve 5), while the intensities of the β-PbO reflections significantly decrease (Fig. 4, curve 7). After calcination at 850 °C, all characteristic reflections in the X-ray diffraction pattern of the sample drastically decrease and the background level significantly increases. This can result even with an increase in dispersity, and even of amorphization.

3.2. SEM

Scanning electron micrographs of the uncalcined material show gibbsite, bayerite, crystal concretions of lead- and lead, aluminium hydroxycarbonates (Fig. 5a) and hydrotalcite (Fig. 5b). No amorphous phases are observed even at high electron microscopic magnifications. Unlike the Mg, Al-hydrotalcite material (Fig. 6a), in the scanning electron micrographs of the 700 °C calcined Pb, Al-hydrotalcite material (Fig. 6b), no amorphization is observed. The small crystallites adhere together forming systems of small channels of diameter 2 nm, and large channels of diameter 5 nm (Fig. 7a). On the walls of the large channels crystals of γ-Al_2O_3 are observed. The walls of the small channels are formed by β-PbO and α-Al_2O_3 crystals (Fig. 7b, c). It appears that decreasing intensity of the α-Al_2O_3 characteristic reflections in the X-ray diffraction pattern of the 700 °C calcined material is a result of increasing dispersity. On the basis of the SEM investigations it can be proposed that the decrease in the intensities of the characteristic reflections of all phases in the X-ray diffraction pattern of

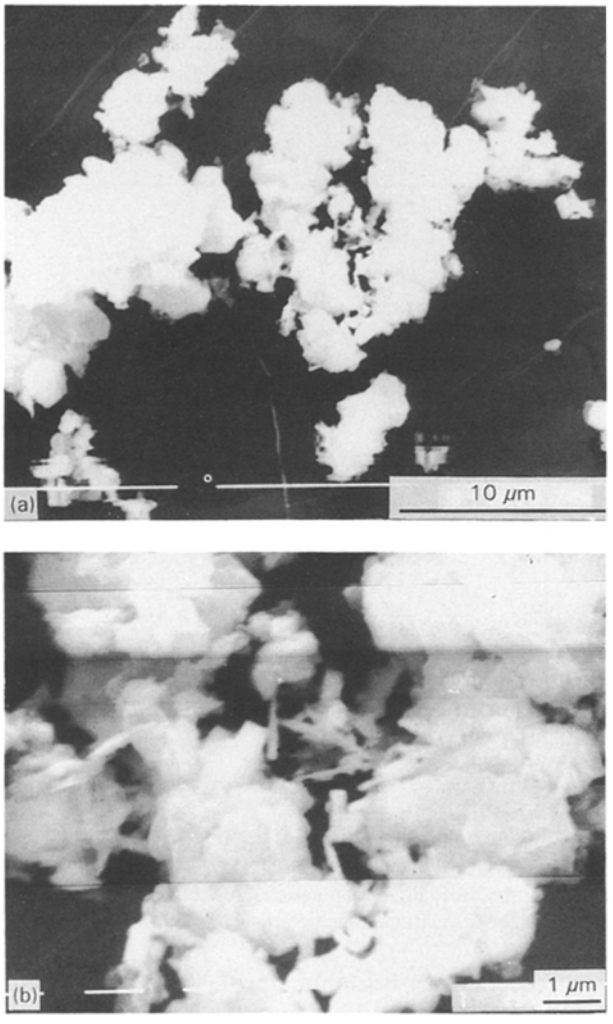

Figure 5 Scanning electron micrographs of the uncalcined Pb, Al-hydrotalcite material (a) × 3500 and (b) × 10 000.

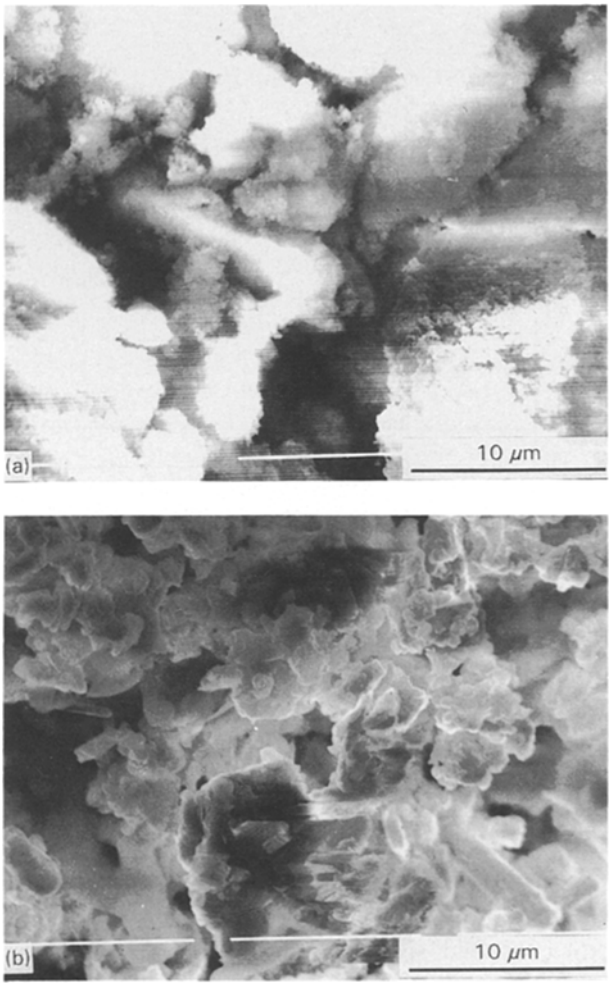

Figure 6 Scanning electron micrographs of the 700 °C calcined (a) Mg, Al-hydrotalcite material and (b) Pb, Al-hydrotalcite material; × 10 000.

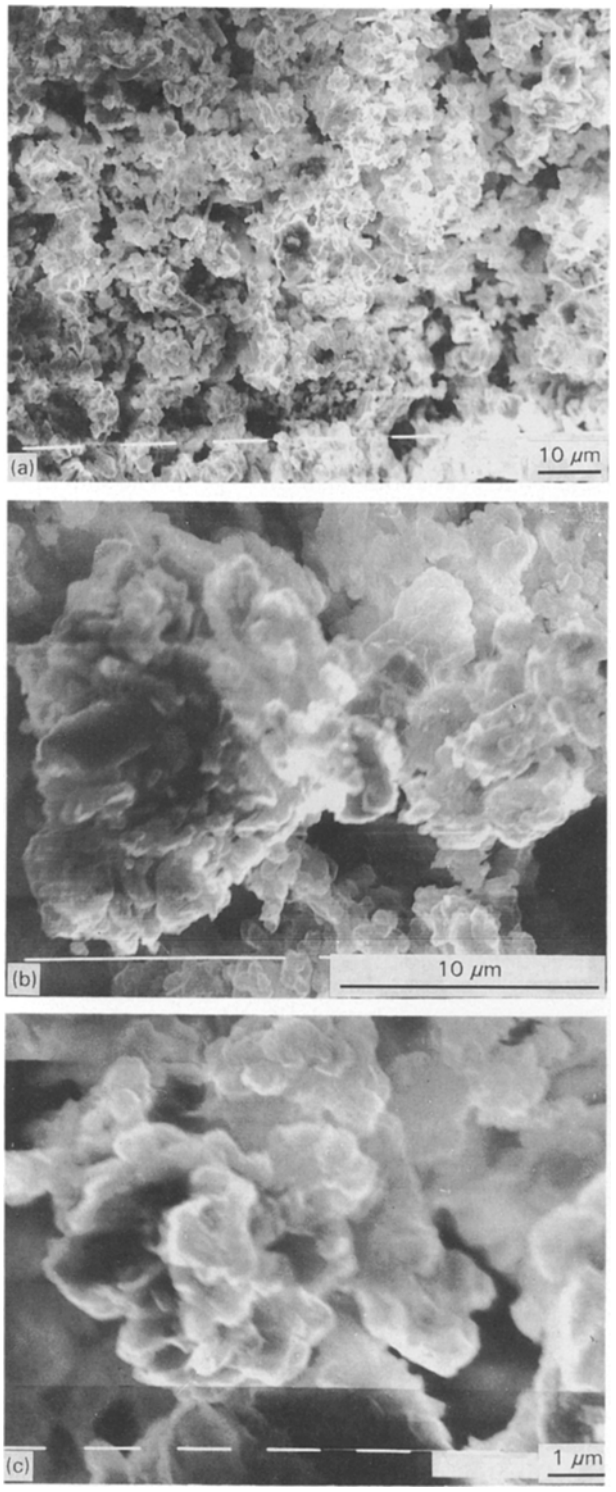

Figure 7 Scanning electron micrographs of 700 °C calcined Pb, Al-hydrotalcite material at (a) × 1000, (b) × 5000, and (c) × 10 000.

the 850 °C calcined material are the result of increased dispersity of the crystallites.

3.3. TEM

The transmission electron micrograph of the uncalcined Pb, Al-hydrotalcite material (Fig. 8a) shows a Japanese twine of hydrotalcite crystals, adhered to a hexagonal bipyramide II {1222}; on the bypiramidal face of one of them a parallel triple concretion of hydrocerrussite is fixed; a crystal concretion of gibbsite is crystallized along the pinacoidal face of the

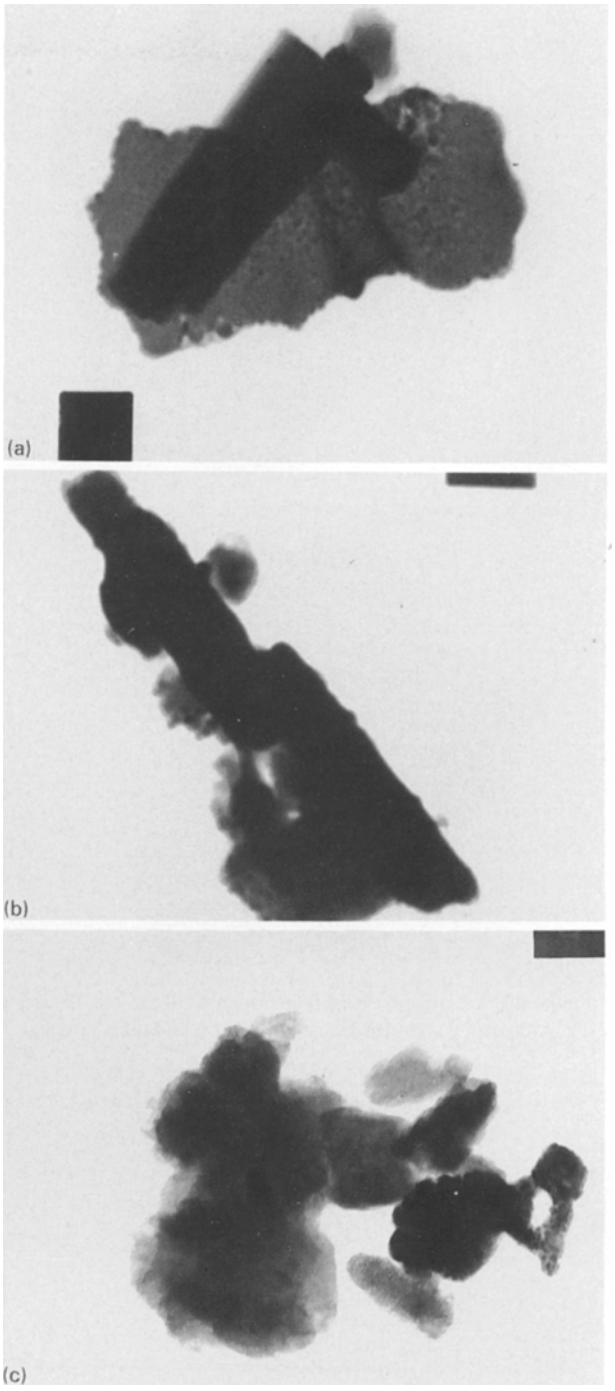

Figure 8 Transmission electron micrographs of the uncalcined Pb, Al-hydrotalcite material at (a) × 50 000, (b) × 70 000 and (c) × 60 000.

hydrocerrussite. Fig. 8b shows a parallel crystal concretion of hydrotalcite in close vicinity to hydrocerrussite, small crystals of dandassite and $Al(OH)_3$. Gibbsite, bayerite, crystal concretions of hydrocerrussite and dandassite in an $Al(OH)_3$ matrix are also seen (Fig. 8c). The transmission electron micrographs of the 700 °C calcined material show β-PbO crystal concretions, forming a well-discernible channel system (Fig. 9a), concretions of α- and γ-Al_2O_3 with a well-developed surface (Fig. 9b).

3.4. IR

Fig. 10 shows the i.r. spectra of the uncalcined Pb, Al-hydrotalcite (spectrum 1) and Mg, Al-hydrotalcite

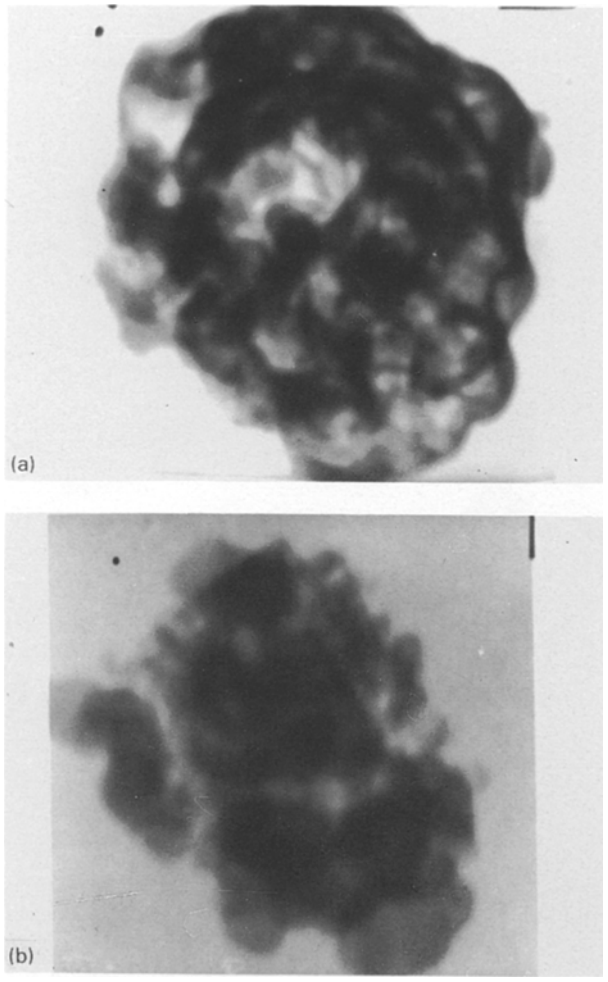

Figure 9 Transmission electron micrographs of the 700 °C calcined Pb, Al-hydrotalcite material at (a) × 50 000 and (b) × 80 000.

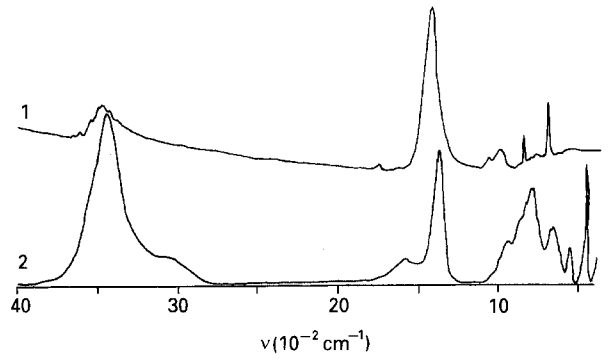

Figure 10 Infrared spectra of the uncalcined (1) Pb, Al-hydrotalcite material and (2) Mg, Al-hydrotalcite material.

(spectrum 2). The weak characteristic bands, corresponding to a hydrotalcite structure observed in the i.r. spectrum of the lead-containing material are shifted to the higher frequency side. The shift can be described by the different ionic radii of Mg^{2+} and Pb^{2+} cations [8].

3.5. DRS

The diffuse-reflectance spectrum of the uncalcined Pb, Al-hydrotalcite material is presented in Fig. 11. The band at about 2260–2240 nm (4424–4464 cm^{-1}) in the spectrum is attributed to the ($\nu + \delta$) vibration of the CO_3^{2-}–H_2O bond [14, 15] in the complexes $[CO_3(H_2O)_4]^{2-}$ fixed in the interlayer distance of the

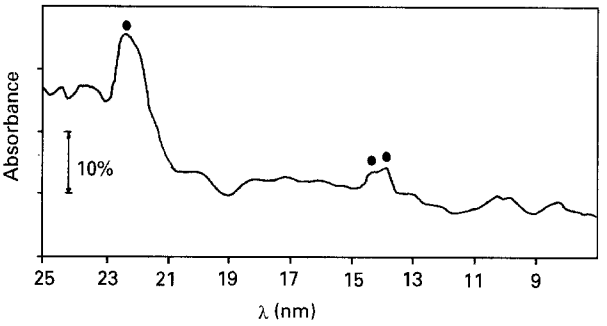

Figure 11 Diffuse-reflectance spectrum of the uncalcined Pb, Al-hydrotalcite material.

hydrotalcite structure [12, 13]. The $\nu_{0\to1}$ vibration of this bond is at about 3050 cm^{-1} [16]. The shift of the band at 4424 cm^{-1} in the spectrum of the hydrotalcite can be the result of CO_3^{2-}–OH bond length alteration as an effect of the interlayer distance alteration in the hydrotalcite structure. The position of this band in the DRS spectrum of the Pb, Al-hydrotalcite material is at 2240 nm, possibly as the effect of the relative decrease in the interlayer distance. In the XRD-pattern of the uncalcined Mg, Al-hydrotalcite material, an interlayer distance of 0.76 nm is detected, while in the XRD pattern of the lead-containing sample, the interlayer distance is 0.67 nm.

The band at 1450 nm (6896 cm^{-1}) corresponds to $\nu_{0\to2}$ O–H bond vibration of $\nu_{0\to1}$ 3525 cm^{-1} in the fragments $[Me^{2+}$–$(O–H)^-$–$Al^{3+}]$ of the hydrotalcite structure [12–16]. The shift of the band at 1450 nm could be the result of O–H bond length alteration in the fragments $[Me^{2+}$–$(O–H^-)$–$Al^{3+}]$ affected by the Me^{2+} ionic radius and electronegativity. This band is shifted to 1430 nm in the spectrum of the lead-containing hydrotalcite. It corresponds to the characteristic O–H bond vibration at 3575 cm^{-1} (seen as a weak band in the i.r. spectrum) in the fragment $[Pb^{2+}$–$(OH)^-$–$Al^{3+}]$ of the Pb, Al-hydrotalcite.

The band at 1380 nm (7246 cm^{-1}) has been attributed [14–16] to $\nu_{0\to2}$ of the characteristic stretching O–H bond vibration (3700 cm^{-1}) of the water molecules, coordinatively bonded to polyvalent cations.

4. Discussion

The results in the present work show that after hydrotalcite synthesize using lead and aluminium precursors, two polymorphous modifications of $Al(OH)_3$ (gibbsite and bayerite) and three lead-containing hydroxycarbonates (dandassite, hydrocerrussite and hydrotalcite) are formed. The small amount of lead-containing hydrotalcite crystals is probably stabilized by the existence of gibbsite and hydrocerrussite in the system. During calcination, the aluminium hydroxides are transformed mainly to γ-Al_2O_3. The dehydration and decarboxylation of the lead-containing components of the material are accomplished at 300 °C, forming a well-developed large-channel system in the calcined sample. The complicated phase transitions of the boehmite and lead oxides above 400 °C, accompanied by dehydration and loss of oxygen, evidently

result from the formation of the small-channel system and crystallization of small crystals of α-Al_2O_3. The calcination of the Pb, Al-hydrotalcite material at 600–750 °C leads to the formation of β-PbO and γ-Al_2O_3. On the basis of the present and previously reported [2, 3] investigations it can be assumed that calcination at 600–750 °C is the best catalytic pre-treatment for the Mg, Pb, Al-hydrotalcite material, at which mainly the catalytically active methane dimerization β-PbO phase is formed in highly dispersed MgO–Al_2O_3 matrix of high basicity.

5. Conclusions

1. By synthesis of hydrotalcite using Reichle's procedure and lead and aluminum nitrates, material is obtained containing gibbsite, bayerite, hydrocerrussite, dandassite and a small amount of Pb, Al-hydrotalcite. The hydrotalcite crystals are stabilized in the presence of gibbsite and hydrocerrusite.

2. The complete dehydration and decarboxylation of the lead-contaning components of the Pb, Al-hydrotalcite material at 300 °C is accompanied by the formation of a well-developed large-channel system in the sample. The small-channel system in the material is formed above 400 °C, during the thermal degradation of boehmite which is accompanied by the release of water ($2AlOOH \rightarrow Al_2O_3 + H_2O$), and the phase transitions of the lead oxides which is accompanied by loss of oxygen ($2PbO_2 \rightarrow PbO + O_2$).

3. The calcination of the Pb, Al-hydrotalcite material at 600–750 °C leads to the formation mainly of β-PbO and γ-Al_2O_3.

4. The calcination of the Mg, Pb, Al-hydrotalcite material at temperatures 600–750 °C is the best catalytic pre-treatment, leading formation of the catalytically active methane dimerization β-PbO phase in a highly dispersed MgO-Al_2O_3 matrix of high basicity.

Acknowledgements

The authors thank the USA National Scientific Foundation (Grant INT-8810539) and National Foundation "Scientific Research" of the Bulgarian Ministry of Education and Science for financial support, and Lt J. Cook for providing the material.

References

1. K. ASAMI, K. HASHIMOTO, K. FUJIMOTO and H.-O. TOMINAGA, in "Methane Conversion", edited by D. M. Bibby (Elsevier Science, Amsterdam, The Netherlands, 1983) p. 403.
2. A. H. WEISS, J. COOK, R. HOLMES, N. DAVIDOVA, P. KOVACHEVA and M. TRAYKOVA, in "Novel Materials in Heterogeneous Catalysis", ACS Symposium Series **437**, edited by L. L. Murrell (ACS, Washington, USA, 1990) Ch. 22, p. 243.
3. M. VALCHEVA-TRAYKOVA, N. DAVIDOVA and A. H. WEISS, *J. Mater. Sci.* **28** (1993) 2157.
4. W. T. RECHLE, *Chem. Technol.* **16** (1986) 58.
5. D. M. ROY, A. ROY and E. F. OSBORN, *Am. J. Sci.* **251** (1953) 337.
6. S. ASBRING and L. NARRBY *Acta Crystallogr.* **B 26** (1970) 8.
7. S. CHOSE, *ibid.* **17** (1964) 1051.
8. I. KOSTOV, in "Mineralogia" (Nauka I Tehnika, Sofia, Bulgaria, 1957) p. 297.
9. G. E. FEKLICHEV, in "Diagnosticheskie spectri Mineralov" (Nedra, Moscow, 1977).
10. N. KACHANOV and L. I. MIRKIN, "Rentgenostrukturnji Analiz-Parkticheskoe rukovodstwo" (MASHGIS, Moscow, 1960) p. 92.
11. I. M. GLISTENKO, "Osnovi nauchnikh issledovanij" (Visha Shkola, Moscow, 1983).
12. R. ALLMANN, *Chimia* **24** (1970) 99.
13. P. G. ROUXNET and H. F. TAYLOR *ibid.* **23** (1969) 480.
14. L. KUSTOV, V. PLASHOTNIK, V. BOROVKOV and V. KAZANSKI, *Kinet. katal.* **23** (!982) 955.
15. V. KAZANSKI, *ibid.* **23** (1982) 1334.
16. L. KUSTOV, V. PLASHOTNIK, V. BOROVKOV and V. KAZANSKI, *ibid.* **23** (1982) 1161.

Received 12 October 1993
and accepted 27 July 1994